

# Finding Computationally Inexpensive Methods to Model the Flow Past Heavy Vehicles and the Design of Active Flow Control Systems for Drag Reduction

David E. Manosalvas\*, Thomas D. Economou\*, Francisco Palacios† and Antony Jameson‡

*Stanford University, Stanford, CA, 94305, USA*

This paper explores the use of computational tools to analyze the aerodynamic effects that Coanda jets have on the drag, stability and maneuverability of heavy vehicles. To facilitate the analysis and understanding of the underlying causes of viscous pressure drag, this paper focuses on the study of the Ground Transportation System (GTS) model.

This study is divided into two stages. The first stage uses two-dimensional geometries to explore the effects that different numerical schemes and Reynolds-Averaged-Navier-Stokes (RANS) turbulence models have on the boundary layer, flow separation, and vortex shedding. The geometries used for this study are a circular cylinder at  $Re = 100,000$  and a square cylinder at  $Re = 22,000$ . This approach was devised to determine the effectiveness of various combinations of numerical schemes and turbulence models for the simulation of highly separated flows while minimizing the computational resources required.

The second stage uses the information available from the two-dimensional bluff body results (first stage) to aid in the selection of the best suited tools to model the aerodynamic characteristics of the GTS model. This section focuses on the use of the best suited combination of numerical scheme and turbulence models to simulate the effect that the use of Coanda jets have on the aerodynamic profile of the GTS model. Finally, simulations of the GTS model equipped with Coanda jets in the trailing end were used to optimize the jet momentum coefficient for drag reduction.

## I. Introduction and Motivation

In the US, the transportation sector is responsible for the consumption of 28% of the total energy produced every year.<sup>1</sup> With the ambitious goal in mind to double the fuel efficiency of new vehicles in the US by 2030,<sup>2</sup> the focus must be shifted towards aerodynamic vehicle design optimization. Heavy vehicles, such as large freight transport trucks and trailers, account for 12-13% of all US petroleum consumption.<sup>3</sup> Due to their heavy usage and standard configuration, these vehicles have become the target for numerous aerodynamic studies focused on drag minimization. The potential for fuel and cost savings is huge: a 12% reduction in fuel use across the national fleet would save 3.2 billion gallons of diesel per year and prevent 28 million tons of CO<sub>2</sub> emissions.<sup>3</sup>

The aerodynamics of heavy trucks are mainly characterized by flow separation and the development of low pressure turbulent wakes.<sup>4</sup> Although great improvements have been made on the tractor with the use of passive techniques, the trailer is responsible for 50-60% of the total drag.<sup>5</sup> The phenomenon caused by the development of a low pressure wake, which causes a higher resistance to motion, is called viscous pressure drag or base drag. Aside from basic streamlining, viscous pressure drag can be reduced by the use of active flow control techniques.<sup>6</sup> Active flow control systems reduce the amount of separation which increases the pressure inside the wake and reduces the overall vehicle drag. Wind tunnel experiments using Coanda jets positioned on the trailing end of a trailer have shown that this type of active flow control system is capable of keeping the flow attached longer and increasing the wake pressure.<sup>6</sup> These types of experiments have

\*Ph.D. Candidate, Department of Aeronautics & Astronautics, AIAA Student Member.

†Engineering Research Associate, Department of Aeronautics & Astronautics, AIAA Senior Member.

‡Thomas V. Jones Professor of Engineering, Department of Aeronautics & Astronautics, AIAA Fellow.

demonstrated not only drag reduction, resulting on a net power savings of more than 15%, but also an improvement in vehicle stability and safety. The latter has been achieved by compensating for the effect of side forces by independently controlling each flow actuator.<sup>4</sup>

Efficient design methods for active flow control will require the computational simulation of highly separated flows. To accurately predict the integrated forces over the GTS is particularly important to be able to model the unsteady flow behavior, vortex shedding frequency, and to obtain an accurate prediction of boundary layer separation. Various studies have been taking place using RANS,<sup>7,8</sup> Large Eddy Simulations (LES),<sup>9</sup> and hybrid RANS/LES methods.<sup>10</sup>

Due to the complexity of the problem, LES has been shown to be the most reliable method when it comes to the predictions of the flow features and integrated forces. Unfortunately, this approach increases the computational requirements significantly, making it prohibitively expensive for use in parametric studies aimed toward the design of drag reduction systems.

In order to be able to use Computational Fluid Dynamics (CFD) for the design of active flow control systems, it is necessary to find a combination of computational tools that will be able to model the behavior of the flow around the GTS model and the influence of active flow control on the integrated forces in a reliable and relatively inexpensive manner.

The purpose of this paper is to present an introductory assessment of the application of industry-standard numerical schemes and turbulence models, and the effectiveness of different combinations to model the aerodynamics of buff bodies. Furthermore, the paper uses the results from simulations over square and circular cylinders to determine the combination of computational tools best suited to model the flow around a GTS model. Finally, the available tools are used to model the effects of placing Coanda jets on the trailing end of the GTS model, and an optimization of the jet momentum coefficient with respect to the vehicle drag is performed.

The paper is laid out as follows. In Section II, a description of the geometrical models and the physical problems for the circular and square cylinders are presented. Furthermore, a summary of the results obtained from the simulations using different combinations of computational tools are shown, and a comparison with the available experimental data takes place. Finally, the best suited tools are selected to be used in the second stage. In Section III, a description of the geometry used for the simulation of the flow around the GTS model is presented. This section includes an overview of the physical problem, the flow conditions, and a description of the computational domain for the GTS and the enhanced GTS models (including the Coanda jets in the trailing end). A brief discussion of the design objective, optimization approach, and the chosen optimization techniques are presented. The numerical results for the flow over the GTS base model and the enhanced GTS model with a variety of momentum coefficients are shown. Finally, Section IV provides a summary of the results and lays out areas and suggestions for future work.

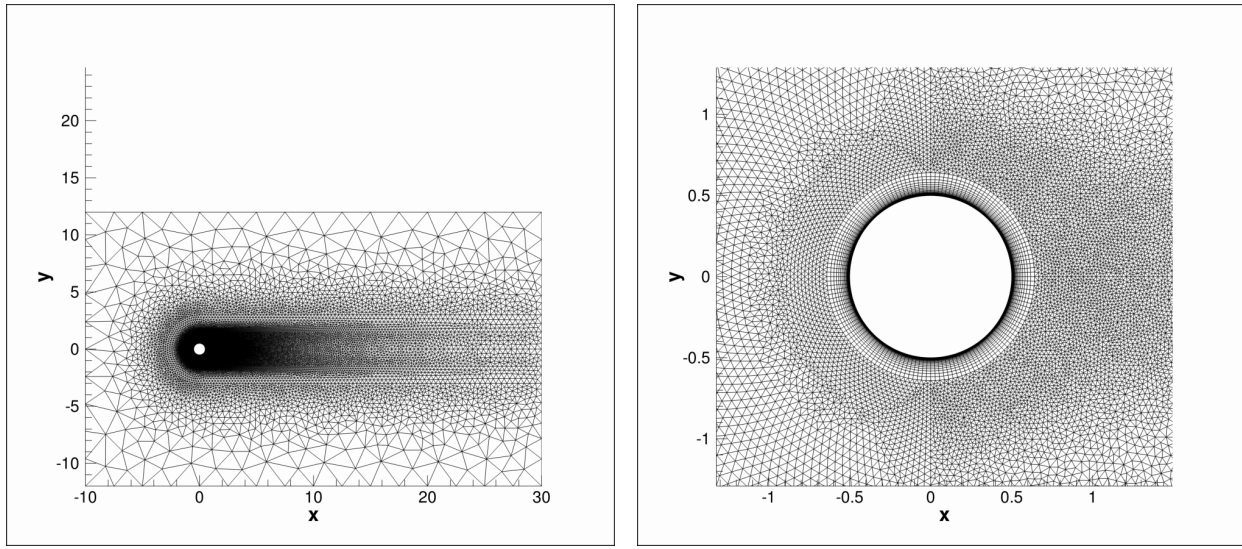
## II. Stage 1: Cylinder Simulations

In order to determine the capabilities of currently available numerical schemes and turbulence models, a case study using circular and square cylinders has been undertaken using the Stanford University Unstructured (SU<sup>2</sup>)<sup>11,12</sup> CFD platform. These geometries were selected due to the geometrical and aerodynamic similarities that they have with respect to each other, as well as with the GTS model. The main reason for having both, square and circular cylinders, is to understand the strengths and weaknesses of the computational tools when dealing with separation from smooth surfaces, as in the circular cylinder, as well as with sharp corners, which are present in the square cylinder. The flow around both geometries at well studied conditions have been simulated and properties including the drag coefficient, separation angle, recirculation region, and Strouhal number have been computed. A comparison with experimental data and other numerical results is used to determine the best combination of computational tools for highly separated flows.

### A. Geometrical and Physical Models

The computational grid for the circular cylinder is composed of 45,766 elements and 25,869 points. The cylinder diameter (D) is one and is used as the characteristic length. The grid is 40D x 20D in the stream-wise and span-wise directions respectively, and the cylinder is positioned at x = 10D. The dimensions of the far-field and the positioning of the cylinder are a modification of the computational domain used by

Catalano *et al.*<sup>13</sup> in 2003. The computational grid is hybrid in nature with a mixture of structured elements near the walls, to better resolve the boundary layer, and unstructured elements to generate a fast growing mesh to the far-field. Figure 1 shows the mesh.

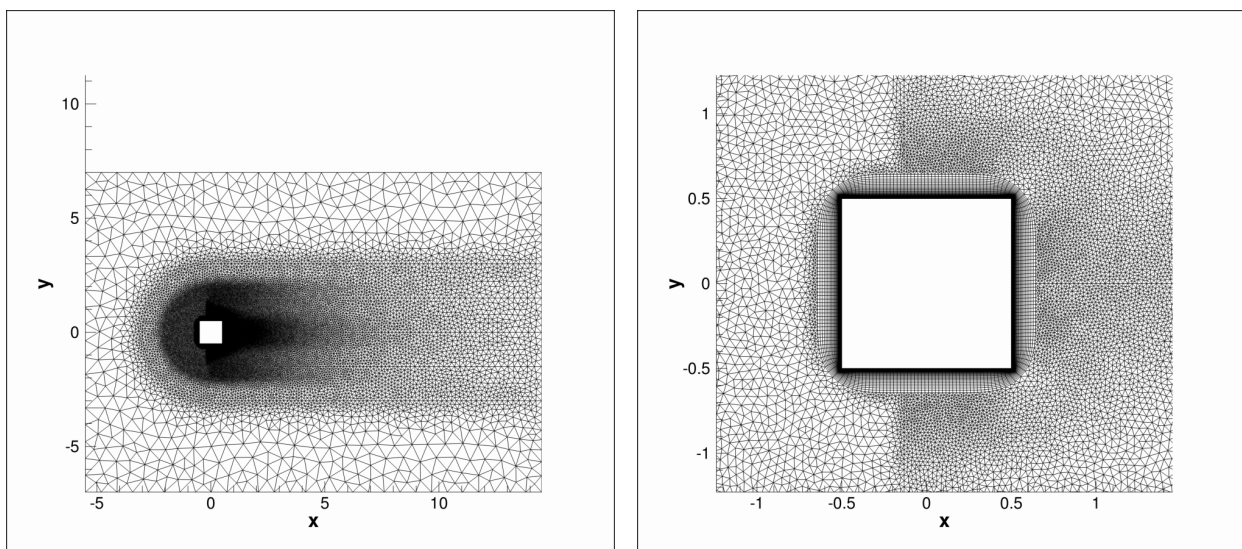


(a) Full domain.

(b) Near-field.

**Figure 1. Views of the computational grid for the circular cylinder.**

For the analysis of this geometry, two second-order numerical schemes have been used for computing the convective fluxes: the Jameson-Schmidt-Turkel (JST)<sup>14</sup> scheme, and the Roe<sup>15</sup> scheme in conjunction with the Venkatakrishnan limiter.<sup>16</sup> These numerical schemes have been used in combination with the Spalart-Allmaras (SA)<sup>17</sup> and Shear Stress Transport (SST)<sup>18</sup> turbulence models. These simulations have been run at a Reynolds number of 100,000 and at a Mach number of 0.1, using a second order numerical scheme and an upwind first-order turbulence model. A dual time stepping scheme has been used for the time integration,<sup>19</sup> using a  $dt = 0.0015s$  to guarantee a well resolved time stencil and the accurate modeling of the periodicity of the system.



(a) Full domain.

(b) Near-field.

**Figure 2. Views of the computational grid for the square cylinder.**

The computational grid used to simulate the flow over a square cylinder is composed of 44,261 elements

and 25,226 points. The height ( $h$ ) is one, and it is used as the characteristic length of the square cylinder. The size of the mesh is  $20h \times 14h$  in the stream-wise and span-wise directions respectively, as recommended by Rodi *et al.*<sup>20</sup> in 1997 and Iaccarino *et al.*<sup>21</sup> in 2003. The square cylinder is located at  $x = 5h$ . The computational grid is hybrid in nature with a mixture of structured elements near the walls, to better resolve the boundary layer, and unstructured elements, to generate a fast growing mesh to the far-field. Figure 2 shows the mesh.

The numerical schemes used for the simulation of the flow over the square cylinder are, once again, JST<sup>14</sup> and Roe<sup>15</sup> combined with the SA<sup>17</sup> and SST<sup>18</sup> turbulence models, as previously described. The square cylinder has been simulated at a Reynolds number of 22,000 and a Mach number of 0.1. A dual time stepping scheme has been used for the time integration,<sup>19</sup> using a  $dt = 0.0015s$ .

## B. Results

The results presented in Tables 1 and 2 are obtained by averaging the flow behavior over 5 periods. The flow visualizations for both the circular and square cylinders shown in Figures 3 and 4 are in good agreement with the experimental and computational results which have been compared.

The obtained results for the circular cylinder from the various cases examined have been summarized in Table 1 alongside the experimental results from Gowen *et al.*<sup>22</sup> in 1953, Roshko<sup>23</sup> in 1961, and Achenbach<sup>24</sup> in 1968.

| <b>Contribution</b>        | <b>Model</b>           | <b><math>Re</math></b> | <b><math>\overline{C_d}</math></b> | <b><math>S_t</math></b> | <b><math>\theta_s</math></b> | <b><math>C_b</math></b> |
|----------------------------|------------------------|------------------------|------------------------------------|-------------------------|------------------------------|-------------------------|
| Gowen <i>et al.</i> , 1953 | Experiments $M = 0.4$  | 100,000                | 1.18 – 1.27                        | –                       | 94°                          | -1.25                   |
| Roshko, 1961               | Experiments $M = 0.25$ | 100,000                | 1.2                                | 0.19 – 0.23             | 85°                          | -1.13                   |
| Achenbach, 1968            | Experiments $M = 0.1$  | 100,000                | 1.0 – 1.2                          | –                       | 78°                          | -1.17                   |
| Present JST                | URANS – SA             | 100,000                | 0.7912                             | 0.2708                  | 86.85°                       | -0.8705                 |
| <b>Present JST</b>         | <b>URANS – SST</b>     | <b>100,000</b>         | <b>0.9827</b>                      | <b>0.2576</b>           | <b>84.84°</b>                | <b>-1.0729</b>          |
| Present ROE                | URANS – SA             | 100,000                | 0.8418                             | 0.2760                  | 90.23°                       | -0.9073                 |
| Present ROE                | URANS – SST            | 100,000                | 0.8807                             | 0.2616                  | 90.64°                       | -1.0208                 |

**Table 1.** Results for the circular cylinder  $M = 0.1$ .  $\overline{C_d}$  is the time-averaged drag coefficient,  $Re$  is the Reynolds number,  $S_t$  is the Strouhal number,  $\theta_s$  is the average angle at which it separates, and  $C_b$  is the pressure coefficient inside the wake of the cylinder.

As expected, the flow past a circular cylinder exhibits separation and periodic vortex shedding. The frequency at which the vortices are being shed is represented by the Strouhal number, which is in good agreement between the combination of computational tools. The computationally obtained Strouhal number is higher than the experimental results by Roshko,<sup>23</sup> and this is in part due to the difference in Mach numbers. The numerical simulations are at the same Reynolds numbers as the results published by Roshko<sup>23</sup> and Gowen *et al.*<sup>22</sup> but a lower Mach number was selected to better represent the flow past a heavy vehicle. These results are included in the table since they provide good insight on the results obtained, and are a good metric for quantifying the effect that the Mach number has on the flow past bluff bodies. The average drag coefficient obtained by the combination of JST<sup>14</sup> and SST<sup>18</sup> is in good agreement with the experimental data presented by Achenbach in 1968,<sup>24</sup> which is particularly relevant to this study since the experiments were performed at the same Reynolds and Mach numbers. The other combinations of numerical schemes and turbulence models underpredict the drag coefficient. The separation point and base pressure coefficient are not well predicted by the numerical simulations. This is to be expected since the available RANS models have not been generated with separated flow applications in mind and have difficulty predicting separation. Even though the results are not in full agreement with the experimental data, it can be seen that the combination of JST<sup>14</sup> and SST<sup>18</sup> most closely agree with the experimental values. The results obtained for the simulation of the flow past a circular cylinder using this combination are presented in Figure 3.

The simulation results for the square cylinder have been compared with experimental data from Lyn *et al.*,<sup>25</sup> Lee,<sup>26</sup> and Vickery,<sup>27</sup> as well as with computational results obtained from Rodi *et al.*,<sup>20</sup> and Iaccarino *et al.*<sup>21</sup> The results can be seen in Table 2.

As expected, the flow past the square cylinder exhibits periodic vortex shedding in its wake. The frequency at which the cylinder's wake is oscillating is represented by the Strouhal number, which overall is in good

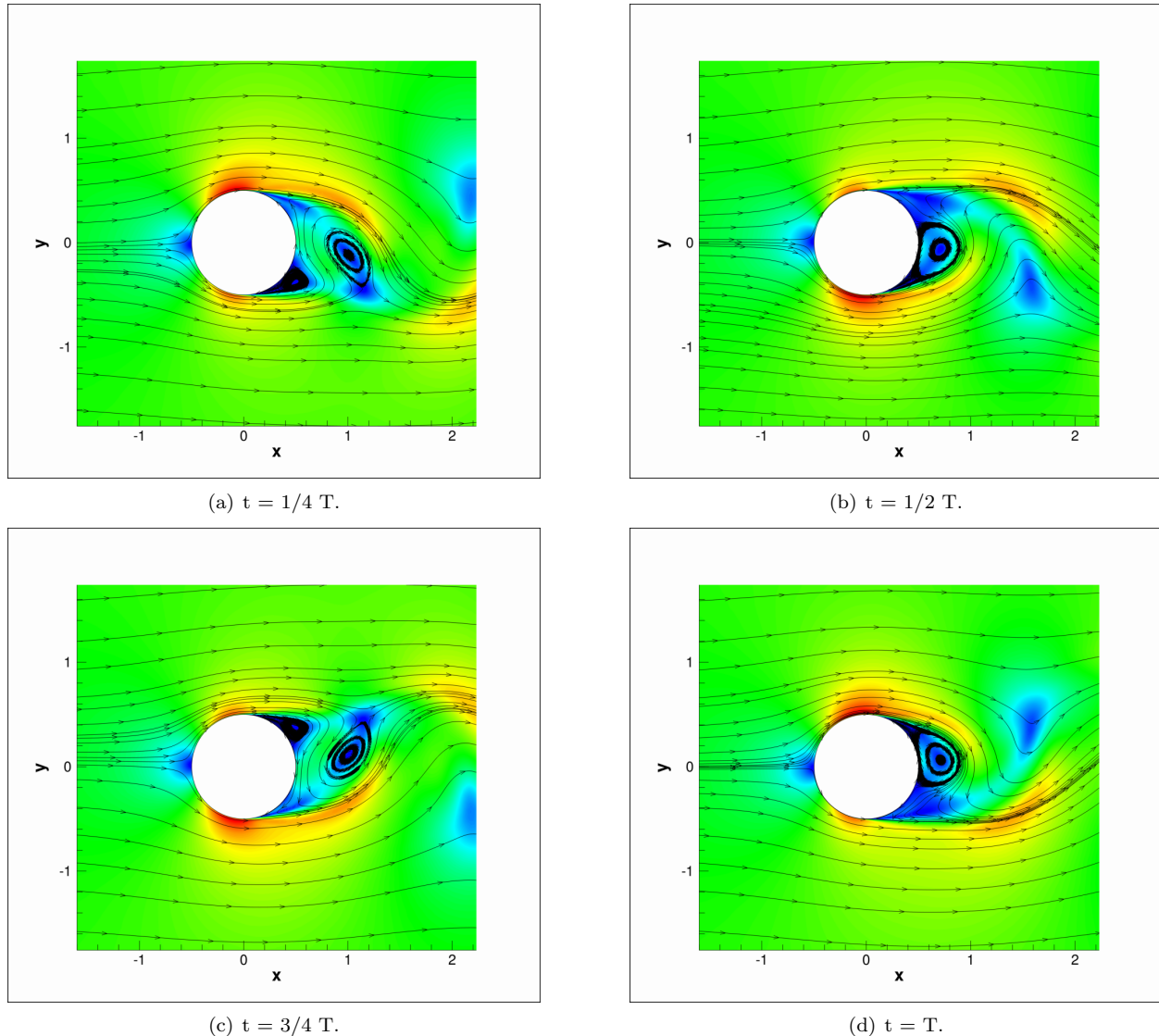


Figure 3. Mach number contours of the time history of the streamlines past a circular cylinder.  $T$  represents one shedding period.

| <b>Contribution</b>            | <b>Model</b>                   | $x_r/h$     | $\bar{C}_d$   | $\tilde{c}_d$   | $\tilde{c}_l$ | $S_t$         |
|--------------------------------|--------------------------------|-------------|---------------|-----------------|---------------|---------------|
| Lyn <i>et al.</i> , 1995       | <i>Experiments</i>             | 1.38        | 2.1           | —               | —             | 0.132         |
| Lee <i>et al.</i> , 1975       | <i>Experiments</i>             | —           | 2.05          | 0.16 – 0.23     | —             | —             |
| Vickery, 1966                  | <i>Experiments</i>             | —           | 2.05          | 0.1 – 0.2       | 0.68 – 1.32   | —             |
| Rodi <i>et al.</i> , 1997      | <i>LES</i>                     | 1.32        | 2.2           | 0.14            | 1.01          | 0.13          |
| Rodi <i>et al.</i> , 1997      | <i>RANS k – ω</i>              | 1.25        | 2.004         | —               | —             | 0.143         |
| Iaccarino <i>et al.</i> , 2003 | <i>URANS v<sup>2</sup> – f</i> | 1.45        | 2.22          | 0.056           | 1.83          | 0.141         |
| <i>Present JST</i>             | <i>URANS – SA</i>              | 1.30        | 2.3760        | 0.04679         | 2.4907        | 0.1382        |
| <b>Present JST</b>             | <b>URANS – SST</b>             | <b>1.31</b> | <b>2.2096</b> | <b>0.005471</b> | <b>1.6835</b> | <b>0.1315</b> |
| <i>Present ROE</i>             | <i>URANS – SA</i>              | 0.89        | 2.4609        | 0.04979         | 2.4680        | 0.1419        |
| <i>Present ROE</i>             | <i>URANS – SST</i>             | 1.03        | 2.2759        | 0.01934         | 1.9473        | 0.1467        |

**Table 2.** Results for the square cylinder at  $Re = 22,000$  and  $M = 0.1$ .  $x_r/h$  is the recirculation length,  $\bar{C}_d$  is the time averaged drag coefficient,  $\tilde{c}_d$  is the drag coefficient variance,  $\tilde{c}_l$  is the lift coefficient variance, and  $S_t$  is the Strouhal number.

agreement with the experimental and computational results found in the literature. This is believed to be the result of the separation point being located at the sharp corners of the square cylinder, which is a major difference from the circular cylinder case.

Looking carefully at all the cases, it can be seen that, just as in the circular cylinder case, the combination of computational tools that agrees most closely with the experimental and LES results is the combination of JST<sup>14</sup> and SST.<sup>18</sup> One of the most important features that has to be analyzed for a square cylinder is the recirculation region behind the cylinder. The recirculation region is formed due to separation, and the value measured ranges widely depending on the selection of computational tools. The general trend with the computational results is to underpredict the length of the recirculation region. The combination of JST<sup>14</sup> and SST<sup>18</sup> simulates the recirculation region with comparable accuracy to the LES results presented by Rodi *et al.* in 1997,<sup>20</sup> and the results are not far from the experimental values presented by Lyn *et al.* in 1995.<sup>25</sup> The drag coefficient and lift coefficient variance are overestimated by these simulations, while the drag coefficient fluctuations are underestimated with respect to the experimental data. A plausible explanation for this disagreement is the lack of three-dimensional effects that are believed to have a great influence in the lift coefficient fluctuations.<sup>21</sup> The results obtained for the simulation of the flow past a square cylinder using the combination of JST<sup>14</sup> - SST<sup>18</sup> are presented in Figure 4.

The results obtained from the circular and square cylinders show that, although there are some limitations on the accuracy to which these computational tools are able to simulate separated flows, the general trends for bluff body aerodynamics are captured, and the results are within an acceptable range for design purposes. The flow features that proved to be the most challenging for the computational tools were: separation angle on the circular cylinder and the recirculation region behind the square cylinder. Based on the overall behavior of the numerical solutions, the combination of JST<sup>14</sup> and SST<sup>18</sup> has proven the most capable for predicting the flow past bluff bodies, and therefore it is the chosen combination for the second stage of this paper.

### III. Stage 2: Active Flow Control for the GTS Model

Heavy vehicles have a variety of features that cause flow separation, such as mirrors, antennas, gaps, mud flaps, etc. To facilitate the study of the underlying causes of viscous pressure drag, a clean model, such as the GTS, has been used.<sup>28</sup> The ungapped GTS model removes all the detailed features including the tractor-trailer gap, height difference, and the wheels. The GTS model effectively combines both the tractor and the trailer into a single, simplified bluff body that has a semicircular leading shape and ends in a sharp straight cut in the back.

#### A. Geometrical Model

For the purpose of this analysis, a similar GTS geometry as the one chosen by Englar<sup>6,29</sup> has been selected.

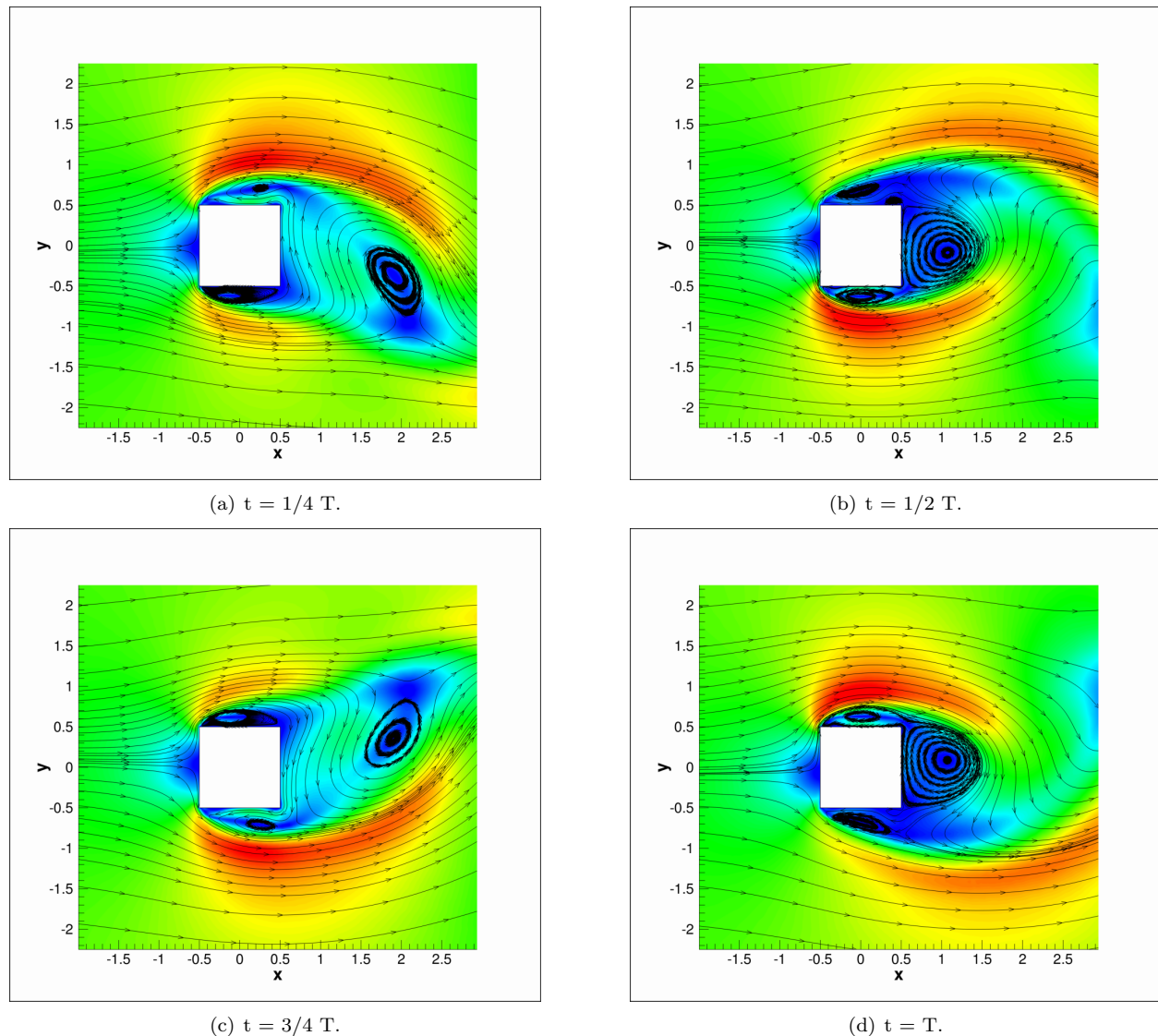


**Figure 4.** Mach number contours of the time history of the streamlines past a square cylinder. T represents one shedding period.

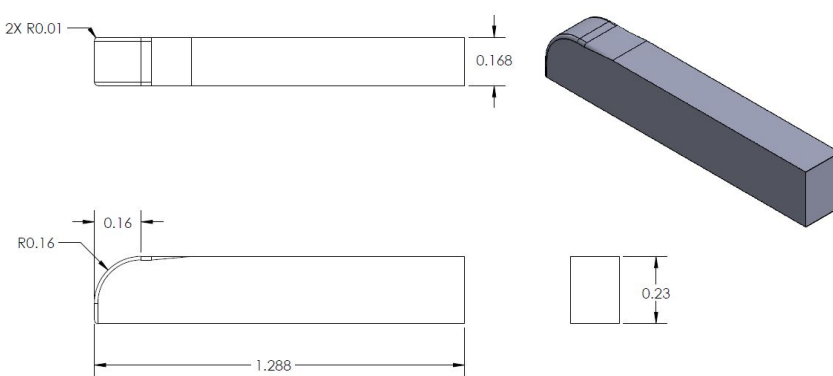


**Figure 5.** Baseline three-dimensional GTS model - Scale 0.065. All dimension are in meters.

In addition to the base model in Figure 5, a model which includes Coanda jets in all four corners of the trailing edge was generated and is shown in Figure 6. The Coanda jet geometry used for this study was chosen based on the experimental results obtained by Englar in 2001.<sup>6</sup>

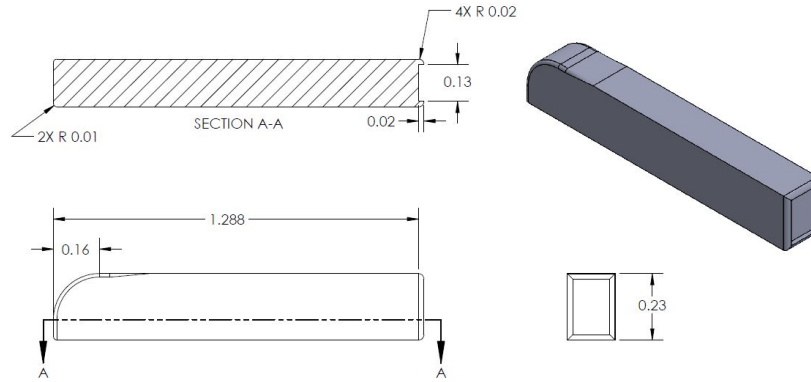


**Figure 6. 3D GTS model with Coanda Jets in the trailing edge - Scale 0.065. All dimension are in meters.**

In order to reduce the computational costs of this study, a two-dimensional model capable of representing the prominent flow features was selected. The principal effects of active flow control that this study aims to analyze are drag reduction, as well as lateral stability. For this purpose, the top view of the GTS model was selected. The two-dimensional geometries are shown in Figure 7.

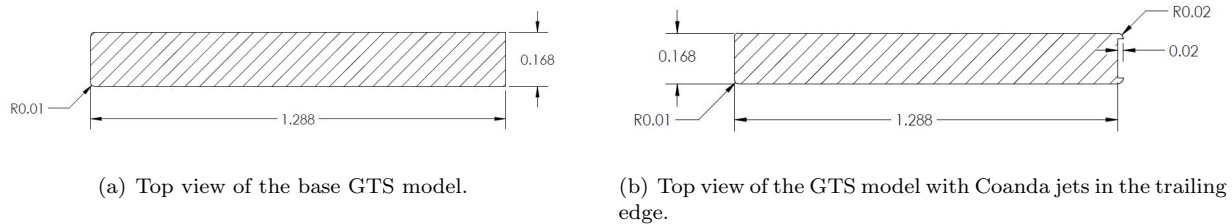


**Figure 7. 2D GTS models- Scale 0.065. All dimension are in meters.**

Although the flow around a ground vehicle has a variety of three-dimensional effects, the two-dimensional top view will allow us to study the effects of the boundary layer, flow separation, and vortex shedding on the drag of the vehicle, as well as the lateral forces induced by the unsteady wake.

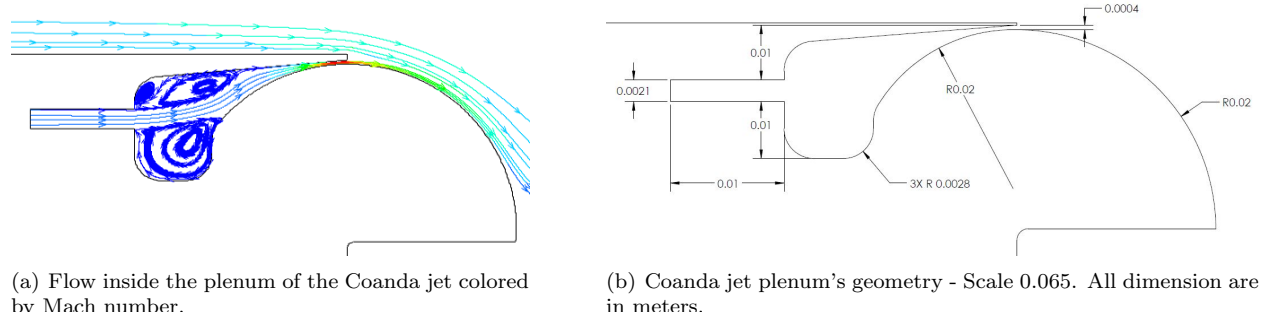


**Figure 8. Model of the Coanda jet.**

To be able to model the flow injection, a plenum-jet interaction had to be included in the geometrical model. For this purpose, inspiration was taken from the Englar airfoil.<sup>30</sup> In general, the chosen plenum shape helps preserve the strain behavior of the flow, which is achieved by generating two standing vortices

that guide the flow towards the Coanda surfaces. The path taken by the flow, and its interaction with the internal vortices, helps reduce the wall effect and allows for a cleaner flow, which helps prevent premature boundary layer separation. Figure 8 shows the Coanda jet geometry and the described flow features.

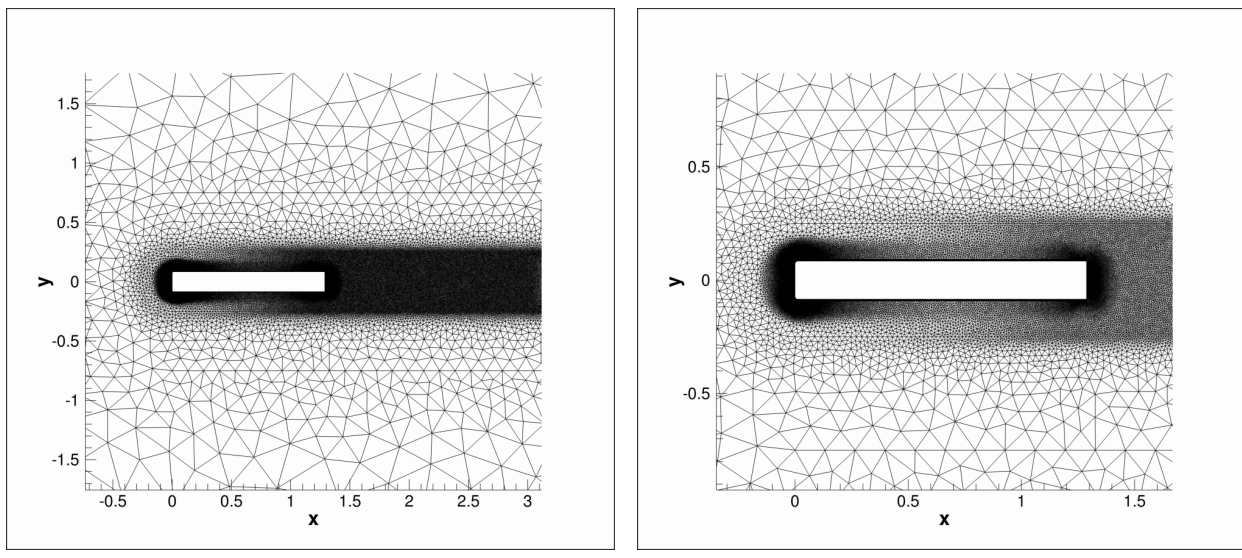
## B. Physical Problem

The GTS model has been analyzed at standard temperature and pressure (STP) conditions, and the velocity chosen was  $31.3 \frac{m}{s}$  (70 mph). For the two-dimensional study, the Reynolds number has been defined as a function of the length of the truck and has been calculated to be 2.75 million. A Mach number of 0.0918 was used. For characterizing the strength of the jet, the drag reduction, and the lateral forces, a momentum coefficient, drag coefficient and lateral force coefficients have been defined as:

$$C_\mu = \frac{\dot{m} * V_e}{q * W}, \quad C_D = \frac{D}{q * W}, \quad C_{LF} = \frac{LF}{q * W}$$

where  $\dot{m}_e$  is the mass flow rate of the jet at the exit,  $V_e$  is the flow velocity at the jet's exit,  $D$  is the drag,  $LF$  is the lateral force,  $q$  is the dynamic pressure calculated as  $\frac{1}{2}\rho_\infty U_\infty^2$ , and  $W$  is the width of the base GTS model.

The two-dimensional domains were discretized using a hybrid mesh, which consists of a structured mesh near the walls, to better capture the boundary layer behavior, and an unstructured mesh towards the farfield, for a more aggressive growth rate while keeping a healthy aspect ratio of the elements. The meshes used, shown on Figures 9 and 10, are  $15L_c$  in length and  $11L_c$  in width. The mesh for the basic GTS model has 88,275 cells and 52,915 points, and the mesh for the enhanced GTS model, which includes the Coanda jets in the trailing edge, has 136,087 cells and 84,837 points. The radical increase in the size of the mesh is due to the addition of the jets. The mesh used to model the Coanda jets is shown in Figure 11.



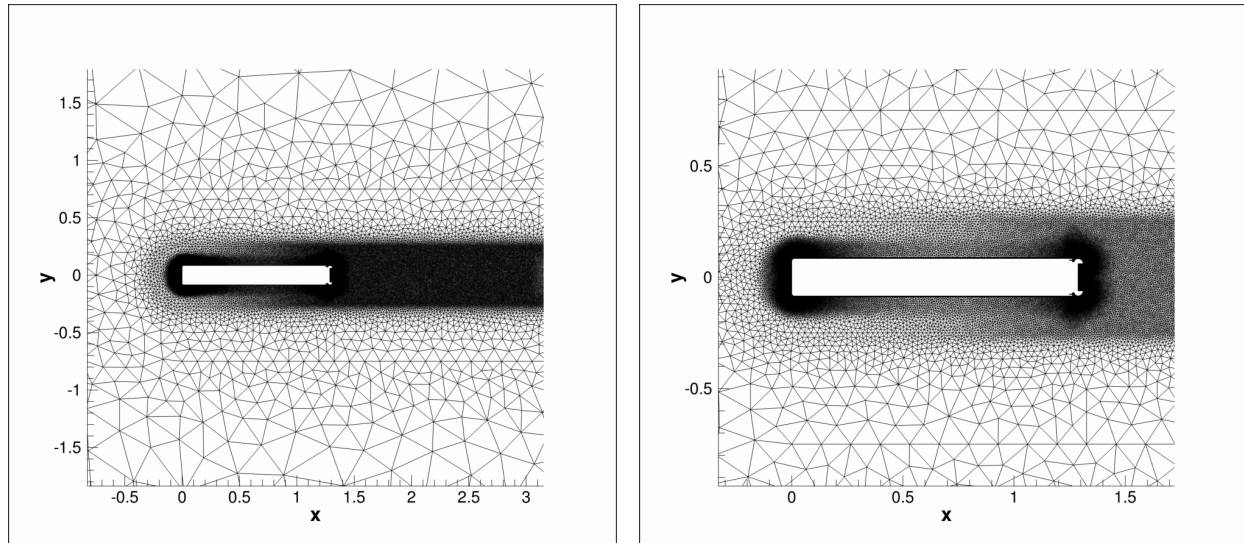
(a) Base GTS mesh including a wake refinement region.

(b) Near-field mesh of the base GTS model.

**Figure 9. Computational grid for the base GTS model.**

## C. Numerical Tools

To model the flow around the base and the enhanced GTS model, the second-order JST<sup>14</sup> numerical scheme combined with the SST<sup>18</sup> turbulence model were chosen. The viscous terms have been computed using a corrected average-gradient method, and two levels of W-cycle multi-grid have been used for convergence enhancement. Time accurate integration was achieved by a dual time stepping approach<sup>19</sup> with a physical time step of 0.0005s and three orders of magnitude of convergence was used at each time step.



(a) Enhanced GTS mesh including a wake refinement region.

(b) Near-field mesh of the enhanced GTS model.

**Figure 10. Computational grid for the enhanced GTS model.**

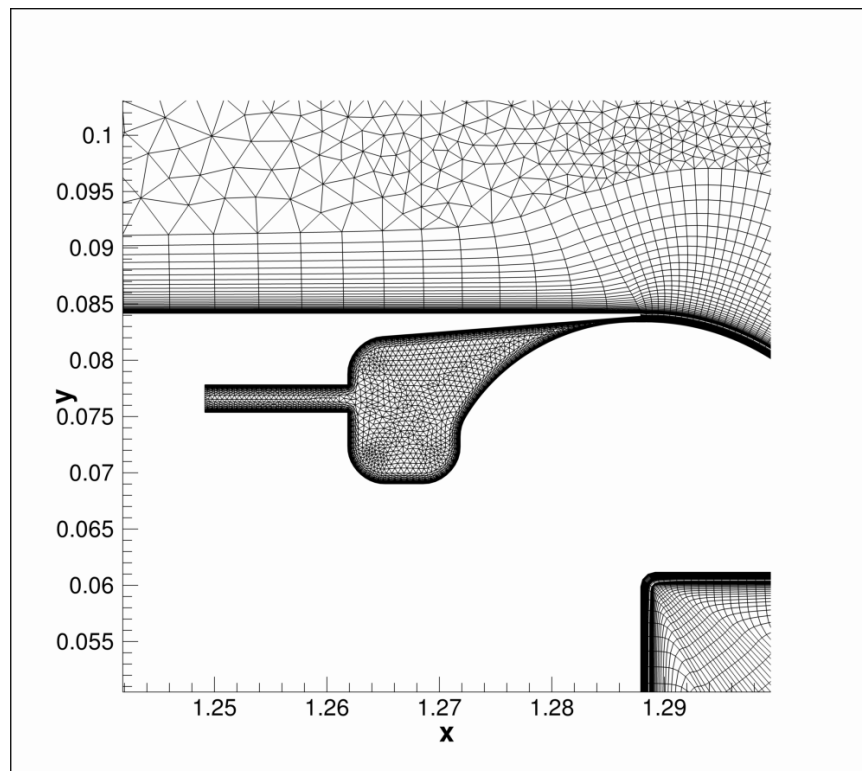


**Figure 11. Computational domain modeling the Coanda jet.**

## D. Active Flow Control Design Methodology

This process focuses on the amount of flow delivered by the Coanda jets, and the energy that this carries, to minimize the drag of the GTS model. The flow delivered by the jet is quantified by the momentum coefficient ( $C_\mu$ ), and the aerodynamic drag on the GTS model is described by the drag coefficient ( $C_D$ ). Due to the unsteady behavior of the aerodynamic profile of the GTS model, and the high computational cost of time accurate integration, a limited amount of function evaluations are available.

To optimize the sampling of  $C_\mu$ , a Gaussian process regression model has been chosen. This approach is used to generate a surrogate model of the system by probabilistically fitting a curve through the points evaluated. Additionally, this technique provides an uncertainty metric, represented by a covariance function<sup>31</sup> which is used to guide the selection of future function evaluations. In this study, an exponential kernel has been used for the covariance function, which is a representation of the standard deviation.

To better guide the prediction, an "expected improvement"<sup>31</sup> function has been implemented. The expected improvement function generates a modified standard deviation distribution. This is achieved by biasing the general standard deviation distribution towards the local minimum of the surrogate model, providing the location at which the minimum is most likely to be found. Each function evaluation brings information to the optimization and modifies the surrogate model making it more accurate.

Based on the work by Englar in 2001,<sup>6</sup> the bounds for the domain have been determined to be between  $C_\mu=0.0$  and  $C_\mu=0.0501$ . The approach chosen to maximize the use of the available computational time was to start by evaluating the cost function at the bounds and at the center ( $C_\mu = 0.0251$ ). Additional sampling of the domain has taken place and a minimum was found after six function evaluations.

## E. Optimization Results

To be able to quantify the improvement obtained by the use of Coanda jets, it was necessary to generate a baseline by simulating the flow over the two-dimensional GTS base model. As expected, the flow over the GTS model exhibits separation, vortex shedding and a periodic turbulent wake. The flow features can be seen in Figure 12. After introducing the Coanda geometry in the trailing edge of the GTS model, a reduction in drag is achieved. This improvement is due exclusively to the geometrical change in the trailing edge of the GTS model. The addition of the Coanda surfaces in the back of the model allows the flow to better negotiate the turn and stay attached longer. This effect can be seen by comparing the flow features in Figures 12 and 13.

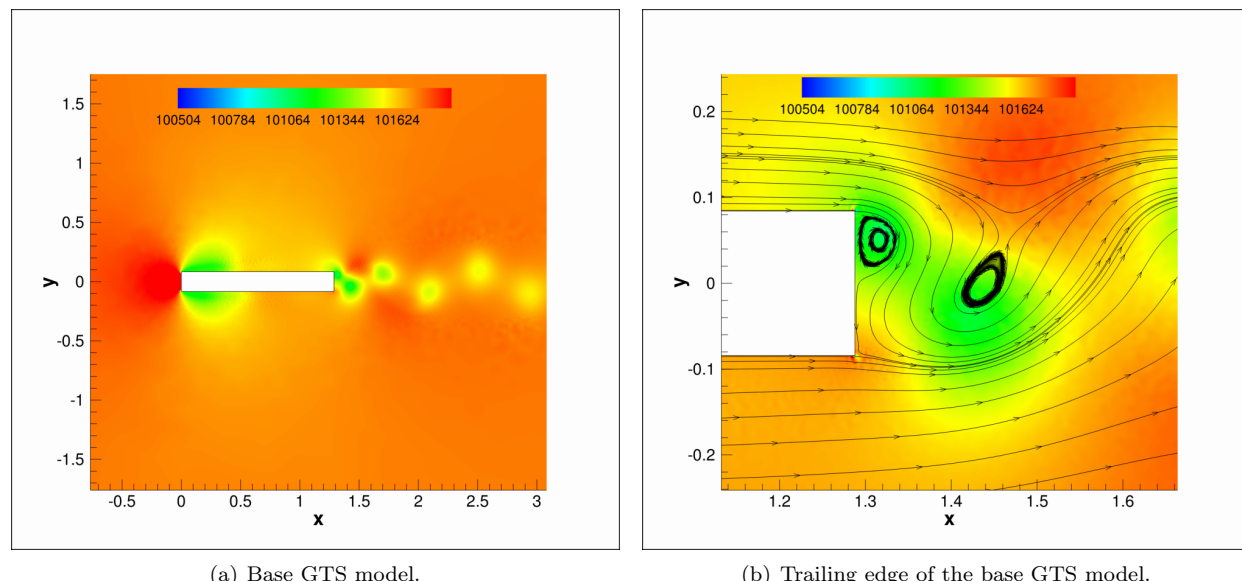
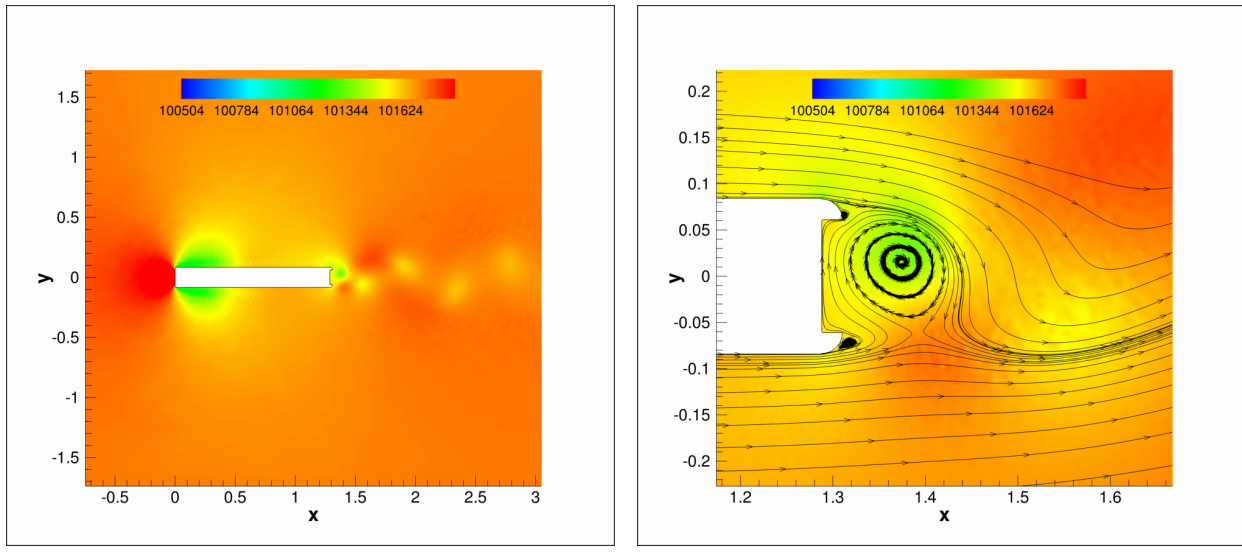


**Figure 12. Pressure contours of the base GTS model. Pressure in Pascals.**

Although the flow stays attached longer with the introduction of the Coanda surfaces, it can be seen that it still separates prematurely. The injection of flow from the jets along the Coanda surfaces introduces



(a) Enhanced GTS model w/o jets. (b) Trailing edge of the enhanced GTS model w/o jets.

**Figure 13. Pressure contours of the enhanced GTS model w/o jets. Pressure in Pascals.**

momentum to the boundary layer, which helps it better negotiate the corners and stay attached longer. The results obtained by following the process outlined in Section III D to choose the different jet momentum coefficients are summarized in Table 3, and the resulting surrogate model is shown in Figure 14.

| $C_\mu$       | Plenum Pressure (Pa) | $\overline{C_D}$ | $\widetilde{C_D}$              | $\widetilde{C_{LF}}$           | $S_t$         |
|---------------|----------------------|------------------|--------------------------------|--------------------------------|---------------|
| —             | —                    | 1.0324           | $9.310E - 05$                  | $6.97E - 02$                   | 0.1801        |
| 0.0000        | 101325               | 0.7707           | $2.860E - 05$                  | $2.86E - 02$                   | 0.1737        |
| 0.0251        | 104070               | 0.6005           | $1.190E - 07$                  | $1.13E - 03$                   | 0.1823        |
| <b>0.0336</b> | <b>105022</b>        | <b>0.5830</b>    | <b><math>4.31E - 08</math></b> | <b><math>6.65E - 04</math></b> | <b>0.1354</b> |
| 0.0346        | 105134               | 0.5838           | $5.80E - 08$                   | $7.10E - 04$                   | 0.1337        |
| 0.0386        | 105582               | 0.5874           | $1.480E - 07$                  | $9.36E - 04$                   | 0.1309        |
| 0.0501        | 106870               | 0.5989           | $7.940E - 07$                  | $2.10E - 03$                   | 0.1345        |

**Table 3. Results for the GTS model and the enhanced GTS model injecting flow through Coanda Jets in the trailing end at momentum coefficients ranging from 0.0 to 0.0501.**  $C_\mu$  is the jet momentum coefficient,  $\overline{C_D}$  is the time averaged drag coefficient,  $\widetilde{C_D}$  is the drag coefficient variance,  $\widetilde{C_{LF}}$  is the lift coefficient variance, and  $S_t$  is the Strouhal number.

From the presented results, it can be seen that the optimum momentum coefficient was found to be at  $C_\mu = 0.0336$ . At this momentum coefficient, not only is the drag coefficient minimized, but also the drag and lateral force coefficient variances. This reduction in the variance comes from a decrease in separation, which in turn dampens the oscillatory behavior of the wake. The Strouhal number, which in the case of the GTS model is a function of the width, is significantly reduced from the base GTS to the enhanced GTS model operating at the optimum momentum coefficient. As the momentum coefficient increases from the optimum position, the Strouhal number remains relatively unchanged – a phenomenon which can be attributed to the amount of separation allowed by the geometry of the Coanda surface and the location at which it is placed on the GTS model. The flow injection at the optimum condition allows the flow to stay attached until the end of the Coanda surfaces, and any further increase in the momentum coefficient has adverse effects on the aerodynamics of the GTS model. The consequences of excess flow injected through the Coanda jet are an increase in the drag coefficient, as well as in the variance of drag and lateral force coefficients. These effects are to be expected, since the excess energy that the jet carries will start to disturb the flow in the wake. Finally, a simple thermodynamic compressor model with an isotropic efficiency of 90% been used to quantify

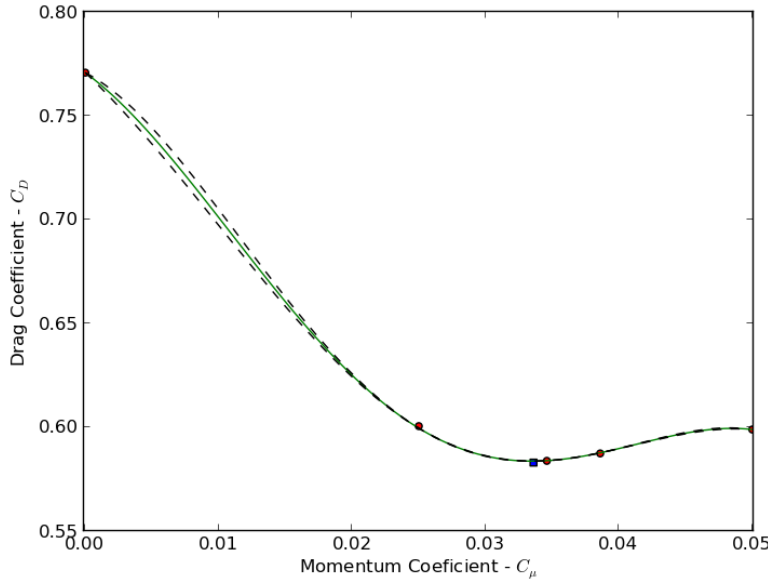


**Figure 14.** Surrogate model for the drag coefficient as a function of the momentum coefficient. The dashed lines represent the uncertainty limit, and the square marker denotes the optimum momentum coefficient.

the required energy to operate the jets. Figure 15 shows both the drag and power coefficients, where the required power is defined as the energy required to overcome the drag of the GTS model plus the energy to power the jets.

$$C_P = \frac{D * U_\infty + P_{compressor}}{q * U_\infty * W}$$

where  $D$  is the drag,  $P_{compressor}$  is the power required to operate the Coanda jets,  $q$  is the dynamic pressure calculated as  $\frac{1}{2}\rho_\infty U_\infty^2$ , and  $W$  is the width of the base GTS model.

The power model was generated to validate the effectiveness of this active flow control system to reduce the energy consumption of the GTS model. As can be seen from Figure 15, an energy reduction is achieved with the use of Coanda jets.

#### IV. Conclusion and Future Work

The selection of a set of simple geometries that can be experimentally validated was essential to determine the best combination of computational tools. The results outlined in the first section of this paper gave us the opportunity to validate the effectiveness of the available numerical schemes and turbulence models for simulating highly separated flows. The combination of the Jameson-Schmidt-Turkel (JST)<sup>14</sup> numerical scheme and Shear Stress Transport (SST)<sup>18</sup> turbulence model proved to be the best suited for the cases analyzed and therefore was used to simulate the flow over the GTS model.

The flow over a two-dimensional GTS model has been numerically computed, and the effects of adding an active flow control drag reduction system composed of Coanda jets have been analyzed. For the analyzed two-dimensional geometries, the addition of the Coanda surfaces had a big effect on the integrated forces, a result that is believed to be due to the lack of three-dimensional effects in the simulation. As the Coanda jet flow is introduced in the simulation the drag is further reduced and the oscillatory nature of the wake is damped. The latter is particularly important to improve stability of the vehicle since the lateral forces influence maneuverability and safety.

To reduce the number of simulations required to find the optimum momentum coefficient a Gaussian process regression was used to generate a surrogate model of the drag coefficient with respect to the momentum

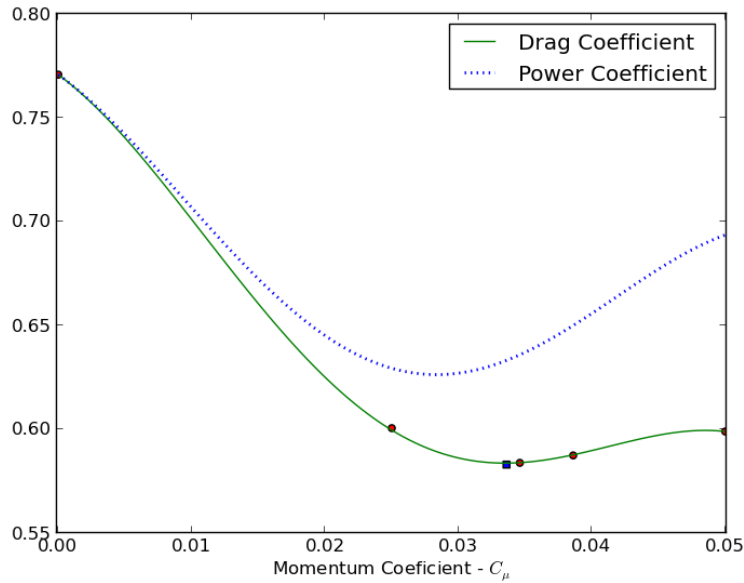


Figure 15. Surrogate model for the drag and power coefficient as a function of the momentum coefficient.

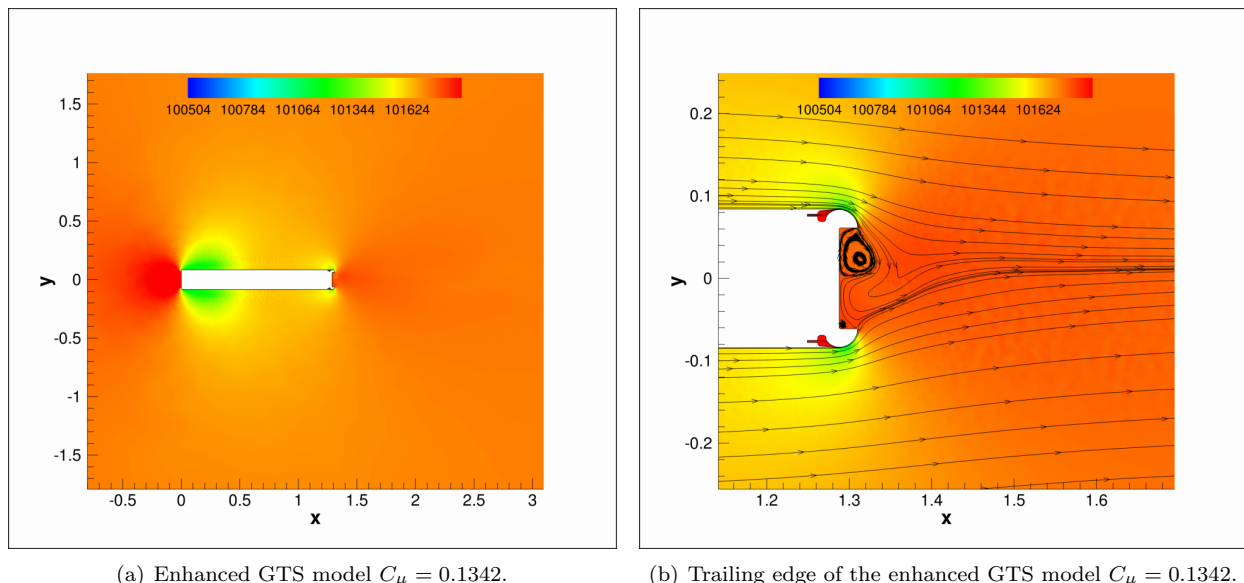


Figure 16. Pressure contours of the enhanced GTS model  $C_\mu = 0.0336$ . Pressure in Pascals.

coefficient, and the expected improvement function was introduced to facilitate the optimization process. The optimum momentum coefficient was found to be at  $C_\mu = 0.0336$ . Although a direct comparison of the two-dimensional results cannot be made, the general trend followed by the integrated forces reported in this paper is similar to the trend followed by the results presented by Englar in 2001.<sup>6</sup> Finally, a power usage model was generated and a decrease on energy consumption has been shown.

Although RANS is not the ideal method for the analysis of highly separated flows, it is imperative to find a combination of methods that are able to mimic the flow over the GTS model inexpensively if we aim to double the fuel efficiency of new vehicles by 2030. The reduction in computational time will not only allow us to perform better parametric and gradient-based studies of drag reduction systems, but will open the door for other design optimization techniques that have the potential to drive the ground transportation sector to a more eco-friendly future.

Moving forward, the emphasis will be placed on the use of shape optimization techniques to better understand the influence that the Coanda surfaces have on the drag coefficient, the Strouhal number, and the variance of the integrated forces. Better understanding the effect that each part of the system causes is essential if we aim to design drag reduction active flow control systems. Since the three-dimensional effects have proven to be significant for this geometry, a detailed analysis of the three-dimensional GTS model will be needed to validate the use of these tools for engineering design.

## V. Acknowledgments

The authors will like to thank the Air Force Office of Scientific Research under Grant FA9550-10-1-0418 for its support, Prof. Mykel Kochenderfer, Prof. Juan Alonso and Trent Lukaczyk for all their guidance in the optimization process; the members of the Aerospace Computing Laboratory and the Aerospace Design Laboratory at Stanford University for many useful discussions; and all the members of the Stanford University Unstructured (SU<sup>2</sup>) development team for their hard work to bring this CFD suite to the open source community.

## References

- <sup>1</sup>US Energy Information Administration. Annual Energy Review. Technical report, 2011.
- <sup>2</sup>Synergistic challenges in data-intensive science and exascale computing. Technical report, DOE ASCAC Data Subcommittee Report.
- <sup>3</sup>K. Salari. DOE's effort to reduce truck aerodynamic drag through joint experiments and computations. Technical report, DOE Annual Merit Review, 2012.
- <sup>4</sup>J. Pfeiffer and R. King. Multivariable closed-loop flow control of drag and yaw moment for a 3D bluff body. In *6th AIAA Flow Control Conference*, 2012.
- <sup>5</sup>P. van Leeuwen. Computational analysis of base drag reduction using active flow control. Master's thesis, TU Delft, 2009.
- <sup>6</sup>R Englar. Advanced aerodynamic devices to improve the performance, economics, handling, and safety of heavy vehicles. *SAE Technical paper series*, 01(2072):1–14, 2001.
- <sup>7</sup>G. Iaccarino, B De Maio, R Verzicco, and B Khalighi. RANS Simulations of Passive and Active Drag Reduction Devices for a Road Vehicle. In *The Aerodynamics of Heavy Vehicles: Trucks, Buses, and Trains*, pages Vol. 19, pp. 267–276. 2004.
- <sup>8</sup>C Roy, J Payne, M McWherter-Payne, and K Salary. RANS Simulation of a Simplified Tractor/Trailer Geometry. In *The Aerodynamics of Heavy Vehicles: Trucks, Buses, and Trains*, pages Vol. 19, pp. 206–218.
- <sup>9</sup>J. Ortega, T Dunn, R McCallen, and K Salari. Computational Simulation of a Heavy Vehicle Trailer Wake. In *The Aerodynamics of Heavy Vehicles: Trucks, Buses, and Trains*, pages Vol. 19, pp. 219–233. 2004.
- <sup>10</sup>F. Menter and M Kuntz. Adaptation of Eddy-Viscosity Turbulence Models to the Unsteady Separated Flow Behind Vehicles. In *The Aerodynamics of Heavy Vehicles: Trucks, Buses, and Trains*, pages Vol. 19, pp. 339–352. 2004.
- <sup>11</sup>F Palacios, M Colombo, A Aranake, A Campos, S Copeland, T Economou, A Lonkar, T Taylor, and J Alonso. Stanford University Unstructured (SU2): An open-source integrated computational environment for multi-physics simulation and design. *AIAA*, pages 1–59, 2013.
- <sup>12</sup>F Palacios, T Economou, A Aranake, S Copeland, A Lonkar, T Lukaczyk, D Manosalvas, K Naik, S Padron, B Tracey, A Variyar, and J Alonso. Stanford University Unstructured (SU2): Open-source Analysis and Design Technology for Turbulent Flows. (2014-0243):1–33, 2014.
- <sup>13</sup>P Catalano, M Wang, G Iaccarino, and P Moin. Numerical simulation of the flow around a circular cylinder at high Reynolds numbers. *International Journal of Heat and Fluid Flow*, 24(4):463–469, August 2003.
- <sup>14</sup>A Jameson, W Schmidt, and E Turkel. Numerical solutions of the Euler equations by finite volume methods using Runge-Kutta time-stepping schemes. *AIAA paper*, M:1–19, 1981.
- <sup>15</sup>P Roe. Approximate Riemann solvers, parameter vectors, and difference schemes. *Journal of computational physics*, 372:357–372, 1981.

- <sup>16</sup>V. Venkatakrishnan. On the accuracy of limiters and convergence to steady state solutions. In *AIAA 31st Aerospace Sciences Meeting & Exhibit*, Reno, NV, 1993.
- <sup>17</sup>P Spalart and S Allmaras. A one-equation turbulence model for aerodynamic flows. *La Recherche Aerospatiale*, 1992.
- <sup>18</sup>F Menter. Two-equation eddy-viscosity turbulence models for engineering applications. *AIAA journal*, 32:1598–1605, 1994.
- <sup>19</sup>A Jameson. Time dependent calculations using multigrid, with applications to unsteady flows past airfoils and wings. In *AIAA 10th Computational Fluid Dynamics Conference*, 1991.
- <sup>20</sup>W Rodi and M Breuer. Status of Large Eddy Simulation : Results of a Workshop. *Fluid Engineering*, 119(June 1997):248–262, 1997.
- <sup>21</sup>G. Iaccarino, A. Ooi, P. Durbin, and M. Behnia. Reynolds averaged simulation of unsteady separated flow. *International Journal of Heat and Fluid Flow*, 24(2):147–156, April 2003.
- <sup>22</sup>F Gowen and E Perkins. Drag of circular cylinders for a wide range of Reynolds numbers and Mach numbers. Technical Report June, National Advisory Committee for Aeronautics, MPfett Field, CA, 1953.
- <sup>23</sup>A Roshko. Experiments on the flow past a circular cylinder at very high Reynolds number. *Journal of Fluid Mechanics*, (1924):345–356, 1961.
- <sup>24</sup>E. Achenbach. Distribution of local pressure and skin friction around a circular cylinder in cross-flow up to  $Re = 5 \cdot 10^6$ . *Journal of Fluid Mechanics*, 34(04):625, March 1968.
- <sup>25</sup>D Lyn. A laser-Doppler velocimetry study of ensemble-averaged characteristics of the turbulent near wake of a square cylinder. *Fluid Mechanics*, 304:205–332, 1995.
- <sup>26</sup>B Lee. The effect of turbulence on the surface pressure field of a square prism. *Journal of Fluid Mechanics*, 69(02):263–289, March 1975.
- <sup>27</sup>J Vickery. Fluctuating lift and drag on a long cylinder of square n a turbulent stream cross-section in a smooth and i. *Fluid Mechanics*, 25:481–503, 1966.
- <sup>28</sup>P van Leeuwen. *Computational Analysis of Base Drag Reduction Using Active Flow Control*. PhD thesis, Delft University of Technology, 2009.
- <sup>29</sup>R Englar. Developmetn of Pneumatic Aerodynamic Devices to Improve the Performance, Economics, and Safety of Heavy Vehicles. *SEA Technical paper series*, 01(2208):1–14, 2000.
- <sup>30</sup>R Englar, G Jones, B Allan, and J Lin. 2-D Circulation Control Airfoil Benchmark Experiments Intended for CFD Code Validation,. *AIAA Paper*, (2009-902):1–27, 2009.
- <sup>31</sup>A. Forrester, A. Sobester, and A. Keane. *Engineering Design Via Surrogate Modelling: A Practical Guide*. Progress in astronautics and aeronautics. Wiley, 2008.